

# Performance modeling of PVT collectors: Implementation, validation and parameter identification approach using TRNSYS



Danny Jonas<sup>a,\*</sup>, Manuel Lämmle<sup>b</sup>, Danjana Theis<sup>c</sup>, Sebastian Schneider<sup>c</sup>, Georg Frey<sup>a</sup>

<sup>a</sup> Saarland University, Chair of Automation and Energy Systems, Saarbrücken, Germany

<sup>b</sup> Fraunhofer Institute for Solar Energy Systems ISE, Freiburg, Germany

<sup>c</sup> htw saar, University of Applied Sciences, Saarbrücken, Germany

## ARTICLE INFO

### Keywords:

Modeling  
Simulation  
Photovoltaic-thermal collectors  
Experimental validation  
TRNSYS

## ABSTRACT

Photovoltaic-thermal (PVT) collectors are hybrid solutions for the conversion of solar energy into electrical and thermal energy. The development of validated and standardized PVT collector models is important for the comparison of products, informed decision making based on energetic and economic performance, and to promote the market diffusion of PVT technology. This contribution presents a novel PVT performance model, compares different parameter identification approaches, and validates the model and its implementation in a common simulation software (TRNSYS) for system simulations.

For the thermal performance model, a two-node model with either one or two thermal capacities is compared. The two-node approach with one thermal capacity represents an extension of the quasi-dynamic solar thermal collector model with the added functionality of the electrical performance. This modeling approach has also proven to be the recommended modeling approach for the investigated PVT collectors in this work. Furthermore, the parameter identification procedure is described in detail and different approaches are compared. It is shown that a combined identification of thermal and electrical model parameters with determination of all thermal and electrical model parameters is the most suitable approach regarding accuracy and processing effort.

To sum up, the presented PVT performance model and the proposed parameter identification procedure achieve a good agreement of simulated and measured thermal and electrical power output for the analyzed PVT collector types and operating conditions. Hence, the model is suitable for dynamic simulation studies and is proposed as standardized performance model for PVT collectors.

## 1. Introduction

Photovoltaic-thermal (PVT) collectors are hybrid solutions converting solar energy in both electrical and thermal energy. The main objective of PVT collectors is to use the large part of unused solar energy in conventional photovoltaic (PV) modules for thermal applications and to enhance the utilization of limited roof area on buildings. The thermal coupling of solar thermal absorbers to the PV cells results in a thermal energy harvesting system for PV (Zondag, 2008). Moreover, the transfer of heat to a fluid leads to a cooling of the PV modules for fluid temperature conditions below the operating temperature of conventional PV modules. As the electrical efficiency of PV cells increases with decreasing cell temperature, cooling the PV cells leads to an enhanced electrical performance in PVT collectors (Skoplaki and Palyvos, 2009). Depending on the PVT type and application, e.g. for the use in heat pump systems, the use of PVT collectors can lead to a better

utilization of the available roof area in buildings and finally an optimized overall solar yield.

In 2018, the International Energy Agency (IEA) Solar Heating and Cooling (SHC) Programme initiated IEA SHC Task 60 on the application of PVT collectors. IEA SHC Task 60 focusses on the application of PVT collectors with the aim to assess existing solutions and to develop new system solutions with advantages in comparison to classical 'side by side installations' of PV and solar thermal collectors. One objective of IEA SHC Task 60 is to improve the performance characterization and modeling of PVT collectors and systems (IEA SHC, 2018). The development of validated and standardized PVT collector models is an important task to allow for a transparent comparison of products, informed decision making based on energetic and economic performance indicators, and in general to promote the market diffusion of the PVT technology (Kramer and Helmers, 2013).

Currently, the thermal performance of solar thermal and PVT

\* Corresponding author.

E-mail address: [danny.jonas@aut.uni-saarland.de](mailto:danny.jonas@aut.uni-saarland.de) (D. Jonas).

<https://doi.org/10.1016/j.solener.2019.09.047>

Received 22 July 2019; Received in revised form 11 September 2019; Accepted 12 September 2019

Available online 19 September 2019

0038-092X/ © 2019 The Authors. Published by Elsevier Ltd on behalf of International Solar Energy Society. This is an open access article under the CC BY license (<http://creativecommons.org/licenses/by/4.0/>).

**Nomenclature***Abbreviations*

GPS	generalized pattern search
HJ	Hooke-Jeeves
IAM	incidence angle modifier
IEA	International Energy Agency
ISO	International Organization for Standardization
MPP	maximum power point
PR	performance ratio
PV	photovoltaic
PVT	photovoltaic-thermal
SHC	solar heating and cooling
STC	standard test conditions
WISC	wind and/or infrared sensitive collectors

*Symbols*

$A$	gross area, $m^2$
$a$	model parameter a for irradiance dependence of PV efficiency calculation, $m^2 W^{-1}$
$b_0$	constant for incident angle modifier IAM, –
$b$	model parameter b for irradiance dependence of PV efficiency calculation, –
$c$	model parameter c for irradiance dependence of PV efficiency calculation, –
$c_1$	heat loss coefficient, $W m^{-2} K^{-1}$
$c_2$	temperature dependence of the heat loss coefficient, $W m^{-2} K^{-2}$
$c_3$	wind speed dependence of the heat loss coefficient, $J m^{-3} K$
$c_4$	sky temperature dependence of long wave radiation exchange,
$c_5, c_{eff}$	effective thermal capacity, $J m^{-2} K^{-1}$
$c_6$	wind speed dependence of the zero loss efficiency (or transmittance-absorptance product in case of $c_6'$ ), $s m^{-1}$
$c_7$	wind speed dependence of long wave radiation exchange, $W m^{-2} K^{-4}$
$c_8$	radiation losses, $W m^{-2} K^{-4}$
$c_{abs}$	effective thermal capacity of the absorber node, $J m^{-2} K^{-1}$
$c_{fl}$	thermal heat capacity of the fluid node, $J m^{-2} K^{-1}$
$c_p$	specific thermal capacity, $kJ kg^{-1} K^{-1}$
$E_L$	long wave irradiance, $W m^{-2}$
$G$	global solar irradiance, $W m^{-2}$
$G_b$	beam solar irradiance, $W m^{-2}$
$G_d$	diffuse solar irradiance, $W m^{-2}$
$I$	current, A
$K_b$	IAM for beam solar irradiance, –
$K_d$	IAM for diffuse solar irradiance, –
$\dot{m}$	mass flow rate of heat transfer fluid, $kg h^{-1}$
$MAE_{el}$	mean absolute error of the electrical power output, W
$MAE_{th}$	mean absolute error of the thermal power output, W
$MAE_{th+el}$	sum of mean absolute error of the thermal and electrical power output, W
$nMAE_{el}$	normalized mean absolute error of the electrical power output, –

$nMAE_{th}$	normalized mean absolute error of the thermal power output, –
$nRMSE_{el}$	normalized root mean square error of the electrical power output, –
$nRMSE_{th}$	normalized root mean square error of the thermal power output, –
$p_{abs}$	absolute pressure of the ambient air, Pa
$P_{el}$	electrical power output, W
$p_{el}$	specific electrical power output, $W m^{-2}$
$PR$	performance ratio, –
$Q_{th}$	thermal energy output, kWh
$\dot{Q}_{th}$	thermal power output, W
$\dot{q}_{absfl}$	specific heat flow from the absorber to the fluid node, $W m^{-2}$
$\dot{q}_{loss}$	specific thermal losses (or gains) due to heat conduction and convection with the ambient air, $W m^{-2}$
$\dot{q}_{rad}$	specific radiative energy gains, $W m^{-2}$
$\dot{q}_{th}$	specific thermal power output, $W m^{-2}$
$RH$	relative humidity, %
$RMSE_{el}$	root mean square error of the electrical power output, W
$RMSE_{th}$	root mean square error of the thermal power output, W
$T$	temperature, °C
$t$	time, h
$U$	voltage, V
$U_{PVT}$	internal heat transfer coefficient from PV cell to fluid, $W m^{-2} K^{-1}$
$u$	wind speed, $m s^{-1}$
$W_{el}$	electrical energy output of PVT collector, kWh
$\beta$	power temperature coefficient of the PV cells, $\% K^{-1}$
$\eta_0$	zero loss collector efficiency, –
$\eta_{el}$	overall electrical efficiency, –
$\theta$	incidence angle of beam radiation, °
$\sigma$	Stefan-Boltzmann constant, $W m^{-2} K^{-4}$
$\tau\alpha$	transmittance-absorptance product, –

*Subscripts*

a	ambient
abs	absorber
cell	cell
el	electrical
fl	fluid
G	global solar irradiance
in	inlet
m	mean
meas	measurement
out	outlet
PVT	photovoltaic-thermal
ref	reference (usually STC) conditions
sim	simulation
T	temperature
th	thermal
tot	total, overall

*Superscripts*

'	performance coefficients of the two-node model with two thermal capacities
---	--

collectors is tested according to the international standard ISO 9806 and the electrical performance of PV modules according to different IEC standards (depending on the module types). A Solar Keymark certification of PVT collectors is also possible with application of specific rules for PVT collectors as described in Annex P5.1 of the Solar

Keymark Scheme Rules (SKN, 2019). At this, the thermal performance test of PVT collectors shall take place with synchronous thermal and electrical generation under maximum power point (MPP) conditions. As the instantaneous thermal and electrical power is interlinked (Hofmann et al., 2010), it is important to further develop performance models

specifically for PVT collectors.

A first PVT performance model was proposed by Florschuetz (1979), who extended the Hottel-Whillier-Bliss equation and coupled the cell and fluid node by a heat transfer coefficient. This approach is most widely used in the literature to model the electrical performance of PVT collectors (e.g. Chow, 2003; Perers et al., 2012; Bilbao and Sproul, 2015). Fritzsche et al. (2014) and Zenhäusern et al. (2015) developed an empirical performance model based on the measurement of the equivalent cell temperature during standardized steady-state performance tests and correlating the equivalent cell temperature with operating conditions. Helmers and Kramer (2013) extended the quasi-dynamic method and developed electrical and thermal performance equations to simultaneously characterize and calculate the electrical and thermal performance during dynamic operating conditions.

All proposed performance models have their specific strengths and weaknesses but there is currently no standardized modelling and testing approach. In this context, the main objective of this paper is the development and validation of a novel PVT collector performance model based on existing modeling approaches using mainly standardized model parameters, which can be implemented in common simulation software like TRNSYS and used for system simulations. In doing so, the performance model may form the basis for PVT collector performance testing and future certification and standardization schemes. Subsequently, this work presents the detailed implementation, validation and parameter identification procedure of the PVT performance model using TRNSYS. The presented PVT performance model is an adaption of the quasi-dynamic thermal collector model of ISO 9806 for PVT collectors with additional modeling of the electrical performance.

In the following sections, the PVT collector modeling (Section 2) and the experimental measurement (Section 3) are described. Afterwards, in Section 4 the procedure and results of the parameter identification with TRNSYS (TRNSYS, 2015) and GenOpt (Wetter, 2016) are presented. This is followed by a discussion of the results in Section 5. Finally, Section 6 provides the main conclusions and an outlook on further work.

## 2. PVT collector modeling

### 2.1. Overview

The main concept of the proposed model is the development of a PVT performance model, which connects the quasi-dynamic thermal collector model of ISO 9806 with a PV performance model via a two-node model approach with internal heat transfer coefficient  $U_{PVT}$  (see Fig. 1). The numerical description is based on the work of Lämmle et al. (2017) and Jonas et al. (2018). The PV performance model is implemented in TRNSYS Type 835 (Jonas, 2018) and can be connected to the ISO 9806 implementation in TRNSYS Type 832 (Haller et al., 2014) for a combined PVT performance model. In addition, TRNSYS Type 835 can be coupled to other existing models of solar thermal collectors or absorbers for the calculation of the electrical power output of WISC (wind and/or infrared sensitive collectors) and covered PVT collectors or can be used as PV model with internal cell temperature calculation.

The electrical performance model considers loss effects of incidence angle, temperature and irradiance. Therein, the PVT cell temperature  $T_{cell}$  is calculated via an equivalent thermal network with the internal heat transfer coefficient  $U_{PVT}$ , which connects the PVT cell temperature to the mean fluid temperature  $T_m$  of the PVT collector (see Fig. 2). The constant parameter  $U_{PVT}$  is characterized by parameter identification during quasi-dynamic or steady-state performance measurements according to ISO 9806. Alternatively,  $U_{PVT}$  can be obtained numerically from the collector efficiency factor  $F'$ , by dark-measurements with surface temperature measurements, or via finite element methods (Lämmle, 2018).

In the following, the thermal performance model of both solar thermal and PVT collectors bases on this two-node model. Two

approaches, which differ by the number of thermal capacities, are compared, followed by a description of the electrical performance model.

### 2.2. Thermal performance model

#### 2.2.1. Two-node model with one thermal capacity

The basic thermal model as two-node thermal model with one effective thermal heat capacity  $c_{eff}$  and with consideration of the temperature node  $T_m$  (mean fluid temperature) can be described by the following differential equation, which is an expression of the energy balance of the temperature node  $T_m$  in Fig. 3a:

$$c_{eff} \cdot dT_m/dt = \dot{q}_{rad} - \dot{q}_{loss} - \dot{q}_{th} \quad (1)$$

where  $\dot{q}_{rad}$  are the specific radiative energy gains (radiative energy balance),  $\dot{q}_{loss}$  the specific thermal losses (or gains) due to heat conduction and convection with the ambient air and  $\dot{q}_{th}$  the specific thermal power output of the collector, which is transferred to the fluid. Within this approach all thermal capacities (e.g. fluid, absorber, frame or insulation) are lumped together in the effective thermal heat capacity  $c_{eff}$  and it is assumed that the temperature of this node is represented by the fluid temperature (Fischer and Müller-Steinhagen, 2009). The thermal power output (useful energy gain) can be defined with the mass flow  $\dot{m}$ , the specific thermal capacity  $c_p$  and the outlet  $T_{out}$  and inlet temperature  $T_{in}$  of the heat transfer fluid relative to the gross collector area  $A_{PVT}$  to:

$$\dot{q}_{th} = \dot{m} \cdot c_p \cdot (T_{out} - T_{in}) / A_{PVT} \quad (2)$$

With the assumption that the long wave radiation does not depend on the collector temperature, the specific radiative energy balance can be expressed with the parameters of ISO 9806 as:

$$\dot{q}_{rad} = \eta_0 \cdot (K_b \cdot G_b + K_d \cdot G_d) + c_4 \cdot (E_L - \sigma \cdot T_a^4) - c_6 \cdot u \cdot G \quad (3)$$

where  $\eta_0$  the zero loss collector efficiency,  $K_b$  the incidence angle modifier (IAM) for beam radiation  $G_b$ ,  $K_d$  the IAM for diffuse radiation  $G_d$ ,  $c_4$  the sky temperature dependence of long wave radiation exchange,  $E_L$  the long wave irradiance,  $\sigma$  the Stefan-Boltzmann constant,  $c_6$  the wind speed dependence of the zero loss efficiency,  $u$  the wind speed in the collector plane and  $G$  the global irradiance in the collector plane.

Furthermore, the specific thermal losses (or gains) can be expressed with the parameters of ISO 9806 as:

$$\dot{q}_{loss} = c_1 \cdot (T_m - T_a) + c_2 \cdot (T_m - T_a)^2 + c_3 \cdot u \cdot (T_m - T_a) \quad (4)$$

where  $c_1$  is the heat loss coefficient,  $c_2$  the temperature dependence of the heat loss coefficient and  $c_3$  the wind speed dependence of the heat loss coefficient.

With Eqs. (3) and (4) and the use of coefficient  $c_5 = c_{eff}$ , Eq. (1) can be transformed to the thermal performance model of the quasi-dynamic collector model from ISO 9806:2013 (ISO 9806, 2013):

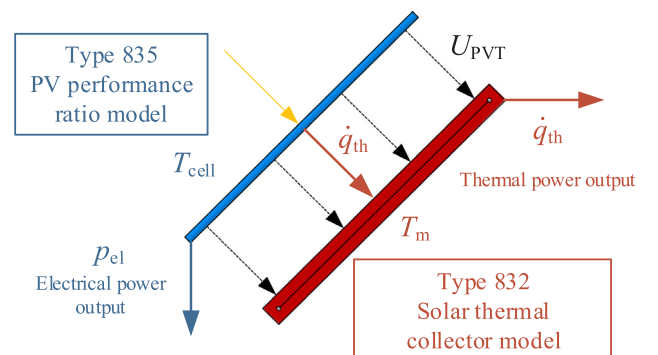


Fig. 1. Coupled PVT model with electrical and thermal performance model.

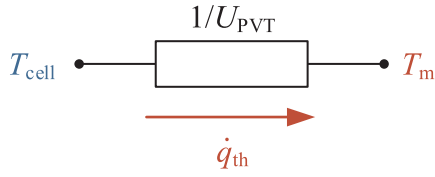


Fig. 2. Equivalent thermal network of the two-node model between temperature nodes  $T_m$  and  $T_{cell}$  interlinked by  $U_{PVT}$ .

$$\begin{aligned} \dot{q}_{th} &= \eta_0 \cdot (K_b \cdot G_b + K_d \cdot G_d) - c_1 \cdot (T_m - T_a) - c_2 \cdot (T_m - T_a)^2 - c_3 \\ &\cdot u \cdot (T_m - T_a) + c_4 \cdot (E_L - \sigma \cdot T_a^4) - c_5 \cdot dT_m/dt - c_6 \cdot u \cdot G \end{aligned} \quad (5)$$

with

$$K_b = 1 - b_{0,th} \cdot [1/\cos(\theta) - 1] \quad (6)$$

where  $b_{0,th}$  is the constant for the thermal incidence angle modifier and  $\theta$  the incidence angle of the beam radiation.

TRNSYS Type 832 (Haller et al., 2014) implements the thermal model with one thermal capacity. For the consideration of ISO 9806:2017 (ISO 9806:2017) Eq. (5) has to be extended by the wind speed dependence of long wave radiation exchange  $c_7$  as well as the radiation losses  $c_8$  and the reduced wind speed  $\bar{u} = u - 3\text{m/s}$  should be used for the modeling. The ISO 9806:2017 model is currently not implemented in TRNSYS Type 832 but could be a good improvement for further development of the model and its use for solar thermal and PVT collector performance characterization with TRNSYS. For this contribution, it was decided to use the ISO 9806:2013 model without reduced wind speed. In addition to the missing implementation of the current standard in Type 832, this was also done in order to obtain physically more comprehensible results that are comparable with parameters previously determined by other test laboratories.

As the electrical mode of operation has a significant impact on the thermal efficiency, it is important that the thermal performance coefficients for the thermal power output calculation of PVT collectors should be determined in MPP mode (Lämmle et al., 2017). The PVT cell temperature  $T_{cell}$  is then calculated as second thermal node without capacitance via the equivalent thermal network with the internal heat transfer coefficient  $U_{PVT}$  which connects the PVT cell temperature with the mean fluid temperature  $T_m$  of the PVT collector. In the following, this approach is called ‘Two-node model with one thermal capacity’. The PVT cell temperature  $T_{cell}$  is then used for the calculation of the cell temperature dependence of the electrical efficiency and the specific

electrical power output  $p_{el}$  (cf. Fig. 3a). The electrical model is described in Section 2.3 and is implemented in TRNSYS Type 835 (Jonas, 2018).

### 2.2.2. Two-node model with two thermal capacities

As alternative to the proposed approach, a second approach will be introduced as ‘two-node model with two thermal capacities’ as it considers the thermal capacitances for each separate node of the mean fluid temperature  $T_m$  and the mean absorber temperature  $T_{abs}$ . For solar thermal collectors, it is known as ‘two-node model’ (Fischer and Müller-Steinhagen, 2009; Theis et al., 2009). Within the thermal two-node model approach, the first energy balance is considered at the  $T_{abs}$  temperature node and the energy balance of the temperature node  $T_{abs}$  can be expressed with the following differential equation:

$$c_{abs} \cdot dT_{abs}/dt = \dot{q}_{rad} - \dot{q}_{loss} - \dot{q}_{absfl} \quad (7)$$

where  $c_{abs}$  is the thermal heat capacity of the absorber and  $\dot{q}_{absfl}$  is the specific thermal energy gain from the absorber to the heat transfer fluid (cf. Fig. 3b). With the assumption that the long wave radiation does not depend on the collector temperature, the specific radiative energy balance can be expressed as:

$$\dot{q}_{rad} = (\tau\alpha) \cdot (K_b \cdot G_b + K_d \cdot G_d) + c_4 \cdot (E_L - \sigma \cdot T_a^4) - c_6 \cdot u \cdot G \quad (8)$$

where  $(\tau\alpha)$  is the transmittance-absorptance product,  $c_4$  the sky temperature dependence of long wave radiation exchange and  $c_6$  the wind speed dependence of the transmittance-absorptance product of the thermal two-node approach.

Furthermore, the specific thermal losses (or gains) can be expressed as:

$$\dot{q}_{loss} = c_1 \cdot (T_{abs} - T_a) + c_2 \cdot (T_{abs} - T_a)^2 + c_3 \cdot u \cdot (T_{abs} - T_a) \quad (9)$$

where  $c_1$  is the heat loss coefficient,  $c_2$  the temperature dependence of the heat loss coefficient and  $c_3$  the wind speed dependence of the heat loss coefficient of the thermal two-node approach. At this, in contrast to the ‘two-node model with one thermal capacity’ in Section 2.2.1, thermal losses are expressed as function of the mean absorber temperature instead of the mean fluid temperature.

With Eqs. (8) and (9), Eq. (7) can be transformed to:

$$\begin{aligned} \dot{q}_{absfl} &= (\tau\alpha) \cdot (K_b \cdot G_b + K_d \cdot G_d) - c_1 \cdot (T_{abs} - T_a) - c_2 \cdot (T_{abs} - T_a)^2 - c_3 \\ &\cdot u \cdot (T_{abs} - T_a) + c_4 \cdot (E_L - \sigma \cdot T_a^4) - c_{abs} \cdot dT_{abs}/dt - c_6 \cdot u \cdot G \end{aligned} \quad (10)$$

A second energy balance is given at the temperature node  $T_m$  with:

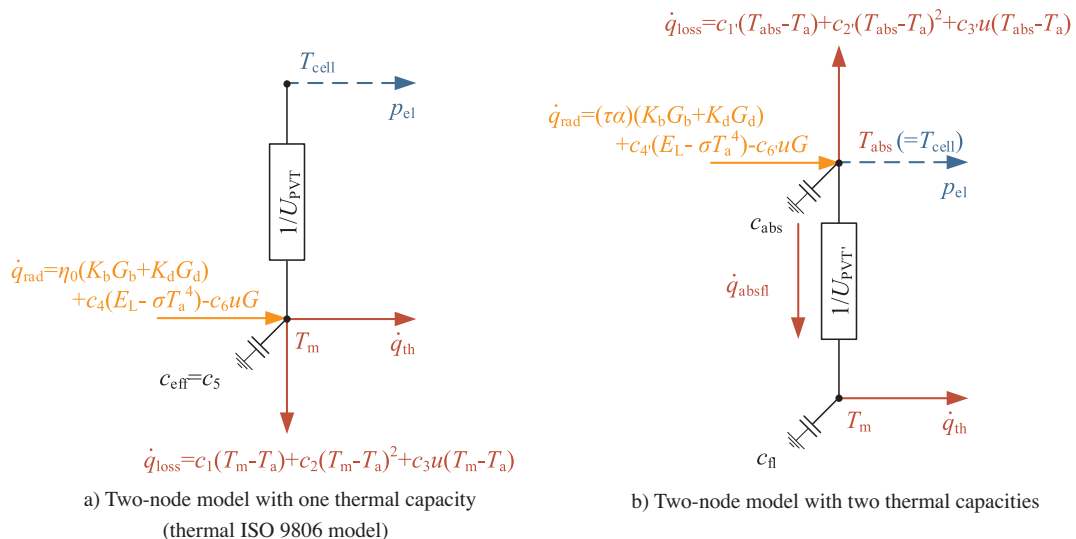


Fig. 3. Thermal network (lumped capacitance model): comparison of two-node model approaches with one or two thermal capacities.

$$c_n \cdot dT_m/dt = \dot{q}_{\text{absfl}} - \dot{q}_{\text{th}} \quad (11)$$

where  $c_n$  is the thermal heat capacity of the fluid (within the collector). The specific thermal energy gain from the absorber to the heat transfer fluid can be defined with the internal heat transfer coefficient  $U_{\text{PVT}}$ , which connects the mean absorber temperature with the mean fluid temperature, to:

$$\dot{q}_{\text{absfl}} = U_{\text{PVT}} \cdot (T_{\text{abs}} - T_m) \quad (12)$$

With Eq. (12), Eq. (11) can be transformed to the equation for the specific thermal power output:

$$\dot{q}_{\text{th}} = U_{\text{PVT}} \cdot (T_{\text{abs}} - T_m) - c_n \cdot dT_m/dt \quad (13)$$

TRNSYS Type 832 (Haller et al., 2014) also implements this two-node model with two thermal capacities. Within this modeling approach, it is also important that the thermal performance coefficients for the thermal power output calculation of the PVT collectors have to be determined in MPP mode. Regarding the calculation of the cell temperature dependence of the electrical efficiency and the specific electrical power output  $p_{\text{el}}$  (described in Section 2.3), the PVT cell temperature  $T_{\text{cell}}$  in this approach is set equal to the calculated mean absorber temperature  $T_{\text{abs}}$  of the PVT collector (cf. Fig. 3b).

### 2.3. Electrical model

The electrical performance model mostly uses datasheet values of PV modules based on characterization according to standard IEC 61853-1 (2011). In addition to the data sheet values, the model requires the earlier mentioned parameter  $U_{\text{PVT}}$  coupling the mean fluid and cell temperature node, for the explicit calculation of the cell temperature (two-node model with one thermal capacity) or the cell temperature is set equal to the mean absorber temperature (two-node model with two thermal capacities).

#### 2.3.1. Overall electrical efficiency and electrical power output

The overall electrical efficiency  $\eta_{\text{el}}$  of the PVT collector in this model is calculated with the performance ratio  $PR_{\text{tot}}$ :

$$\eta_{\text{el}} = \eta_{\text{el,ref}} \cdot PR_{\text{tot}} \quad (14)$$

The electrical power output of the PVT collector  $P_{\text{el}}$  is given by:

$$P_{\text{el}} = \eta_{\text{el,ref}} \cdot PR_{\text{tot}} \cdot G \cdot A_{\text{PVT}} \quad (15)$$

and the specific electrical power output by:

$$p_{\text{el}} = \eta_{\text{el,ref}} \cdot PR_{\text{tot}} \cdot G \quad (16)$$

where  $\eta_{\text{el,ref}}$  is the electrical efficiency at reference conditions (usually STC conditions),  $PR_{\text{tot}}$  is the overall instantaneous performance ratio,  $G$  the global radiation on PVT plane and  $A_{\text{PVT}}$  the gross PVT collector area.

The overall instantaneous performance ratio is calculated with:

$$PR_{\text{tot}} = PR_{\text{IAM}} \cdot PR_G \cdot PR_T \quad (17)$$

The electrical performance model takes the following loss effects (performance ratios  $PR$ ) into account:

- loss effects of incidence angle  $PR_{\text{IAM}}$
- loss effects of irradiance  $PR_G$
- PV cell temperature dependence of electrical efficiency  $PR_T$ .

#### 2.3.2. Loss effects of incidence angle

The instantaneous performance ratio due to incidence angle losses  $PR_{\text{IAM}}$  is calculated with (Duffie and Beckman, 2013):

$$PR_{\text{IAM}} = 1 - b_{0,\text{el}} \cdot [1/\cos(\theta) - 1] \quad (18)$$

where  $b_{0,\text{el}}$  is the constant for electrical IAM and  $\theta$  the incidence angle of beam radiation.

#### 2.3.3. Loss effects of irradiance

The instantaneous performance ratio due to irradiance losses  $PR_G$  is calculated with (Heydenreich et al., 2008):

$$PR_G = a \cdot G + b \cdot \ln(G + 1) + c \cdot [(\ln(G + e))^2 / (G + 1) - 1] \quad (19)$$

with the model parameters  $a$  in  $\text{m}^2 \text{W}^{-1}$ ,  $b$  and  $c$  dimensionless, the global irradiance  $G$  in  $\text{W m}^{-2}$  and the Euler's number  $e$ .

#### 2.3.4. PV cell temperature dependence of the electrical efficiency

The PV cell temperature dependence of the electrical efficiency is calculated with (Skoplaki and Palyvos, 2009):

$$PR_T = 1 - \beta \cdot (T_{\text{cell}} - T_{\text{ref}}) \quad (20)$$

where  $\beta$  is the power temperature coefficient of the PV cells,  $T_{\text{cell}}$  the temperature of the PV cells and  $T_{\text{ref}}$  the PV cell temperature at reference conditions (usually STC conditions).

#### 2.3.5. PVT cell temperature

As described in Section 2.2, the calculation of the PVT cell temperature differs between the two proposed thermal performance models: The two-node model with one thermal capacity calculates  $T_{\text{cell}}$  with a simple equivalent thermal network with an internal heat transfer coefficient  $U_{\text{PVT}}$  which connects the PVT cell temperature  $T_{\text{cell}}$  with the mean fluid temperature  $T_m$  of the PVT collector:

$$T_{\text{cell}} = T_m + \dot{q}_{\text{th}} / U_{\text{PVT}} \quad (21)$$

where  $\dot{q}_{\text{th}}$  is the specific thermal power output of the PVT collector relative to the gross collector area, and  $T_m$  the mean fluid temperature as average of inlet and outlet temperature  $T_{\text{in}}$  and  $T_{\text{out}}$ . In the two-node model with two thermal capacities, the cell temperature is set equal to the mean absorber temperature  $T_{\text{cell}} = T_{\text{abs}}$ .

This novel electrical performance model is implemented in TRNSYS Type 835 (Jonas, 2018) and can be connected to the thermal ISO 9806 TRNSYS model Type 832 (Haller et al., 2014). The IAM parameter  $b_{0,\text{el}}$  can be either identified by a parameter identification process with measurements or set equal to the thermal IAM  $b_{0,\text{th}}$ . The electrical parameters  $\eta_{\text{el,ref}}$  and  $\beta$  can be obtained from the datasheets of the PV modules. The irradiance-dependent parameters  $a$ ,  $b$  and  $c$  are usually determined by a parameter identification of Eq. (19) based on performance measurements according to standard IEC 61853-1 (2011). Since measurement data regarding this standard is rarely provided by manufacturers, literature data, e.g. from Lämmle et al. (2017), can be used as assumption for the modeling of the irradiance behavior.

A comparison of the described electrical performance model with a four-parameter (single diode) PV model, presented in Jonas et al. (2018), figured out that the implementation of a four-parameter PV model has no noticeable advantages for the simulation of the electrical power output in case of the analyzed PVT collectors and operating conditions. Hence, further investigations with a four-parameter (single diode) PV model are not subject of this work.

## 3. Experimental measurements and test sequences

The experimental measurements were realized on an outdoor test bench in Saarbrücken, Germany at the Laboratory for Solar Energy Systems of the University of Applied Sciences htw saar (cf. Fig. 4). Two different types of PVT collectors were installed on a test roof and monitored under dynamic outdoor conditions during MPP operation:

- PVT A – uncovered PVT collector with rear collector cover and thermal insulation material on the back of the PVT absorber, also classified as wind and/or infrared sensitive collector (WISC).
- PVT B – covered PVT collector with front glazing, rear collector cover and no thermal insulation material on the back of the PVT absorber.



Fig. 4. Outdoor test facilities with the investigated PVT collectors.

Besides the standard measurements of the thermal performance according to ISO 9806:2017, the relevant electrical values were measured continuously. A systematic scheme of the measurement set-up including the main measured values used for the performance characterization of the PVT collectors is given in Fig. 5.

According to ISO 9806:2017 the following typical days have to be included in the measurement datasets for thermal performance characterization:

- Day type 1:  $\eta_0$ -conditions, mostly clear sky conditions
- Day type 2: elevated operating temperature or  $\eta_0$ -conditions, partly cloudy conditions including broken cloud and clear sky conditions
- Day type 3: mean operating temperature conditions including clear sky conditions
- Day type 4: high operating temperature conditions including clear sky conditions.

For a better representation of the thermal behavior of the PVT collectors over the entire operating temperature range, two different temperature differences to the ambient  $T_m - T_a$  were measured for day type 3 for PVT A and PVT B. Furthermore, it was possible to operate PVT B with a higher temperature difference to the ambient, due to the lower thermal losses of the covered PVT collector (PVT B). Hence, in case of PVT B a second temperature difference to the ambient was measured for day type 4. The assignment of the measurements to the different operating temperatures of the PVT collectors is given in Table 1.

For the identification of the model parameters for the PVT collectors, the measured test data were evaluated and usable test sequences were separated. For each day type and each type of PVT collector, one sequence was chosen and the sequences were combined to one data set. Within the combined test sequences, a Boolean value is defined for each time step as indicator whether the time step should be considered for the parameter identification or not. The objective of this process is the filtering of start-up sequences between the sequences of different day types and invalid data, e.g. if something was changed in the test bed or measured values are outside a reliable or usable range. To remove unsuitable data, the datasets were filtered to a set of constraints ( $G < 100 \text{ W/m}^2$ ;  $\dot{q}_{th}, p_{el} < 0 \text{ W/m}^2$ ;  $p_{el}, G_d > G$ ;  $T_m < (T_a - 3\text{K})$ ) considering the requirements of each day type. Data points at which at least one of the constraints is violated are disregarded for the calculation of the objective function for the parameter identification process. In addition, it is necessary to remove data points manually, e.g. malfunctions of the MPP tracker, and exclude these data generously from the calculation of the objective function to ensure that the effects of the failure were balanced out again.

## 4. Parameter identification and model validation

### 4.1. Parameter identification procedure with TRNSYS and GenOpt

Identification of model parameters by comparing and adjusting simulated results to measured data is a well-known procedure for different applications, especially in the field of solar thermal systems. In general, an objective function is defined to assess the agreement of the model results with the measured data. The model parameters are then adjusted to better fit the measurement by minimizing the objective function. In the field of solar thermal collectors and systems, the most common methods for the minimization process are multiple linear regression (MLR), which has been introduced as extended version by Perers (1997), and a dynamic parameter identification procedure with the fit program DF (Spirkl, 1997) which uses the Levenberg-Marquardt algorithm (Fischer et al., 2012). Furthermore, newer approaches like Budig et al. (2009) or Almeida et al. (2014) use GenOpt (Wetter, 2016) in combination with TRNSYS for the parameter identification. GenOpt is a generic optimization program which is used to minimize an objective function that is evaluated by an external simulation program like TRNSYS. GenOpt includes a library with different local and global one-dimensional and multi-dimensional optimization algorithms, like Particle Swarm Optimization (meta-heuristic population-based algorithm, stochastic) or Hooke-Jeeves algorithm (GPS-HJ, generalized pattern search method, deterministic). Using these optimization algorithms, specified model parameters are varied systematically in order to minimize the objective function.

In this work, two approaches for the parameter identification of PVT collectors are presented:

- Separated fit: two-step approach with separated thermal and electrical parameter identification procedure
- Combined fit: one-step approach with combined thermal and electrical parameter identification procedure.

The two-step approach with separated thermal and electrical parameter identification procedure for the PVT collector model is shown in Fig. 6. A set of measured values is used as time dependent input for the TRNSYS simulation via a data reader. The measured inputs ( $E_L, G, G_d, \theta, T_a, RH_a, p_{abs}, u, \dot{m}, T_{in}$ ) are then used to simulate the thermal and electrical outputs of the TRNSYS model, especially the thermal  $\dot{Q}_{th,sim}$  and the electrical  $P_{el,sim}$  power output of the PVT collector. Subsequently, the calculated thermal outputs are compared via the absolute error and filtered according to the constraints described in Section 3.

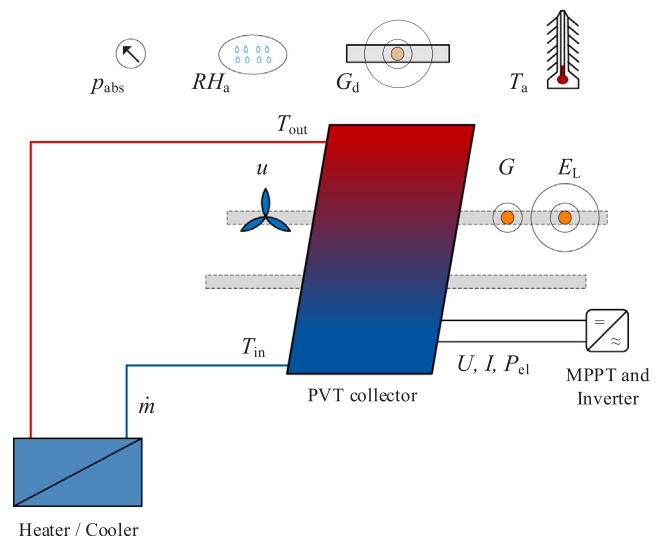


Fig. 5. Measurement scheme of the outdoor test.

**Table 1**  
Performed measurements over the operating temperature range of the PVT collectors.

Day type	1	2	3a	3b	4a	4b
$T_m - T_a$	0 K	0 K or higher	10 K	15 K	20 K	30 K
PVT A	X	X	X	X	X	
PVT B	X	X	X	X	X	X

This is followed by the calculation of the thermal objective function which has to be minimized. In this iterative procedure, GenOpt is used to systematically vary the thermal collector parameters ( $\eta_0$ ,  $K_d$ ,  $b_{0,th}$ ,  $c_1$ - $c_6$  for the two-node model with one thermal capacity) until the minimum of the thermal objective function is reached. The identified set of thermal parameters are then used as fixed parameters for the electrical parameter identification of  $U_{PVT}$  and  $b_{0,el}$ . The described procedure is then repeated in order to minimize the electrical objective function and identify the set of electrical parameters.

In the one-step approach with combined thermal and electrical parameter identification, a combined thermal and electrical objective function is minimized by systematically varying the thermal and the electrical PVT collector parameters simultaneously (cf. Fig. 7).

In addition, the identification of all electrical model parameters including  $U_{PVT}$ ,  $b_{0,el}$ ,  $\eta_{el,ref}$ ,  $\beta$ ,  $a$ ,  $b$  and  $c$  was also integrated in the two-step and one-step approach (see Section 4.3.3).

#### 4.2. Definition of objective function

The mean absolute error (MAE) of the thermal and electrical power output is used as objective function for the parameter identification.

For the two-step approach, the MAE of the thermal power output is used as thermal objective function and the MAE of the electrical power output as electrical objective function:

$$MAE_{th} = \frac{1}{n \cdot \Delta t} \sum_{i=1}^n (|\dot{Q}_{th,sim} - \dot{Q}_{th,meas}| \cdot \Delta t) \tag{22}$$

$$MAE_{el} = \frac{1}{n \cdot \Delta t} \sum_{i=1}^n (|P_{el,sim} - P_{el,meas}| \cdot \Delta t) \tag{23}$$

For the one-step approach with combined thermal and electrical parameter identification procedure, the sum of the MAE of the thermal and electrical power is used as objective function:

$$MAE_{th+el} = \frac{1}{n \cdot \Delta t} \sum_{i=1}^n (|\dot{Q}_{th,sim} - \dot{Q}_{th,meas}| \cdot \Delta t + |P_{el,sim} - P_{el,meas}| \cdot \Delta t) \tag{24}$$

For further analysis of the model accuracy, the normalized mean absolute errors (nMAEs), the root mean square errors (RMSEs) and the normalized root mean square errors (nRMSEs) are defined as:

$$nMAE_{th} = MAE_{th} / \left[ \frac{1}{n \cdot \Delta t} \sum_{i=1}^n (\dot{Q}_{th,meas} \cdot \Delta t) \right] \tag{25}$$

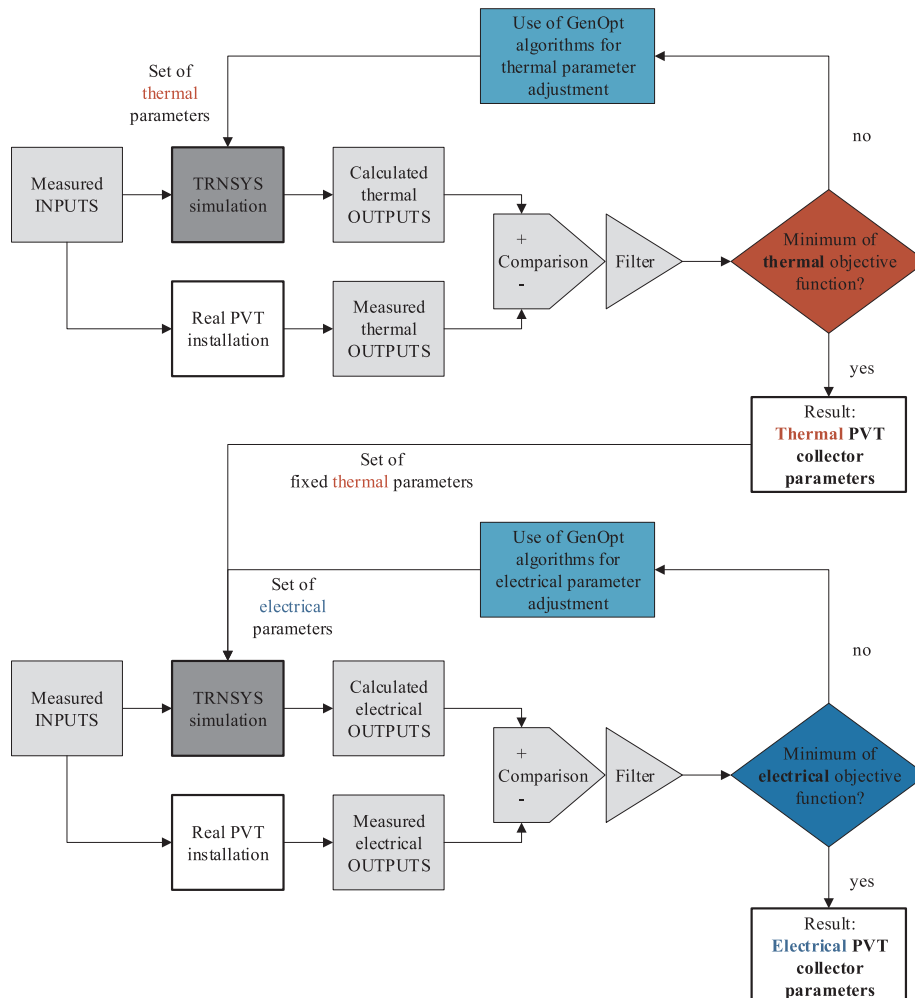


**Fig. 6. Separated fit:** two-step approach with separated thermal and electrical parameter identification procedure.

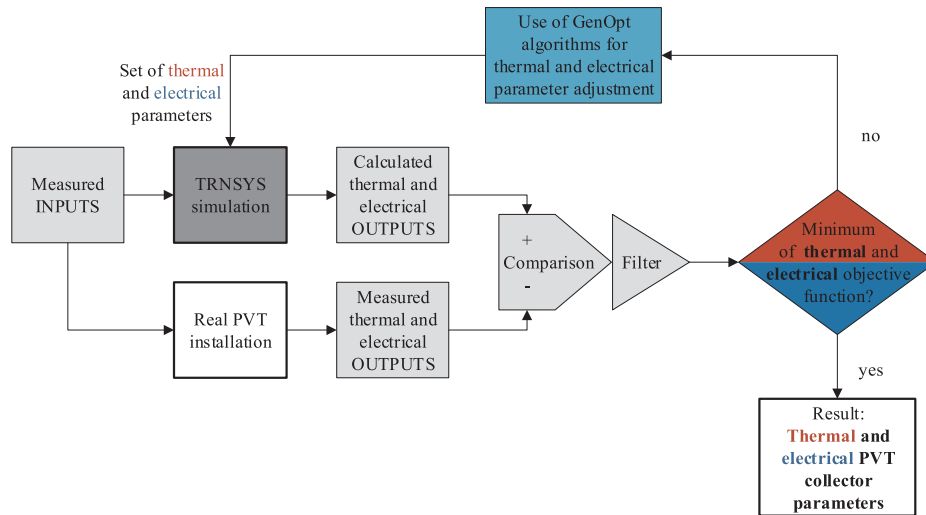


Fig. 7. Combined fit: one-step approach with combined thermal and electrical parameter identification procedure.

$$nMAE_{el} = MAE_{el} / \left[ \frac{1}{n \cdot \Delta t} \sum_{i=1}^n (P_{el,meas} \cdot \Delta t) \right] \quad (26) \quad RMSE_{el} = \sqrt{\frac{\sum_{i=1}^n [(P_{el,sim} - P_{el,meas})^2 \cdot \Delta t]}{n \cdot \Delta t}} \quad (28)$$

$$RMSE_{th} = \sqrt{\frac{\sum_{i=1}^n [(\dot{Q}_{th,sim} - \dot{Q}_{th,meas})^2 \cdot \Delta t]}{n \cdot \Delta t}} \quad (27) \quad nRMSE_{th} = RMSE_{th} / \left[ \frac{1}{n \cdot \Delta t} \sum_{i=1}^n (\dot{Q}_{th,meas} \cdot \Delta t) \right] \quad (29)$$

Table 2  
Results of the parameter identification for PVT A.

PVT A - WISC									
Two-node model w/ one thermal capacity						Two-node model w/ two thermal capacities			
Parameter	Unit	Two-step approach		One-step approach		Parameter	Unit	One-step approach	
		electrical data sheet values	fit of electrical parameters	electrical data sheet values	fit of electrical parameters			electrical data sheet values	fit of electrical parameters
$A_{PVT}$	m <sup>2</sup>	1.66 <sup>1</sup>	1.66 <sup>1</sup>	1.66 <sup>1</sup>	1.66 <sup>1</sup>	$A_{PVT}$	m <sup>2</sup>	1.66 <sup>1</sup>	1.66 <sup>1</sup>
$\eta_0$	-	0.530	0.530	0.531	0.532	$\tau\alpha$	-	0.691	0.576
$K_d$	-	0.914	0.914	0.918	0.920	$K_d$	-	0.890	0.900
$b_{0,th}$	-	0.032	0.032	0.026	0.019	$b_{0,th}$	-	0.052	0.036
$c_1$	W/(m <sup>2</sup> K)	8.104	8.104	8.043	8.018	$c_1'$	W/(m <sup>2</sup> K)	10.328	8.736
$c_2$	W/(m <sup>2</sup> K <sup>2</sup> )	0.023	0.023	0.025	0.029	$c_2'$	W/(m <sup>2</sup> K <sup>2</sup> )	0.087	0.054
$c_3$	J/(m <sup>2</sup> K)	1.7195	1.7195	1.7236	1.7175	$c_3'$	J/(m <sup>2</sup> K)	2.3625	1.9660
$c_4$	-	0.268	0.268	0.286	0.303	$c_4'$	-	0.374	0.296
$c_5$	J/(m <sup>2</sup> K)	37838	37838	37794	37925	$c_{abs}$	J/(m <sup>2</sup> K)	4550	6500
						$c_{fl}$	J/(m <sup>2</sup> K)	19900	18400
$c_6$	s/m	0.031	0.031	0.031	0.031	$c_6'$	s/m	0.028	0.027
$U_{PVT}$	W/(m <sup>2</sup> K)	31.15	46.69	31.18	46.08	$U_{PVT}'$	W/(m <sup>2</sup> K)	35.90	64.40
$b_{0,el}$	-	0.060	0.042	0.060	0.041	$b_{0,el}$	-	0.077	0.045
$\eta_{el,ref}$	-	0.1507 <sup>1</sup>	0.1297	0.1507 <sup>1</sup>	0.1497	$\eta_{el,ref}$	-	0.1507 <sup>1</sup>	0.1517
$\beta$	%/K	0.440 <sup>1</sup>	0.389	0.440 <sup>1</sup>	0.386	$\beta$	%/K	0.440 <sup>1</sup>	0.367
$a$	m <sup>2</sup> /W	-0.00007341 <sup>2</sup>	-0.00012823	-0.00007341 <sup>2</sup>	-0.00008411	$a$	m <sup>2</sup> /W	-0.00007341 <sup>2</sup>	-0.00009461
$b$	-	-0.03588 <sup>2</sup>	-0.01188	-0.03588 <sup>2</sup>	-0.03388	$b$	-	-0.03588 <sup>2</sup>	-0.03588
$c$	-	-1.387 <sup>2</sup>	-1.413	-1.387 <sup>2</sup>	-1.367	$c$	-	-1.387 <sup>2</sup>	-1.371
Results of objective functions									
MAE <sub>th</sub>	W	13.82	13.82	13.83	13.84			12.74	12.86
MAE <sub>el</sub>	W	2.52	2.35	2.51	2.36			2.71	2.39
MAE <sub>th+el</sub>	W	16.34	16.17	16.34	16.20			15.45	15.25

<sup>1</sup>Values were obtained from the data sheets of the manufacturer.

<sup>2</sup>Values have been determined by a parameter fit of Eq. (19) in Microsoft Excel using measurement data according to standard IEC 61853-1 provided by the manufacturer.

$$nRMSE_{el} = RMSE_{el} / \left[ \frac{1}{n \cdot \Delta t} \sum_{i=1}^n (P_{el, meas} \cdot \Delta t) \right] \tag{30}$$

Instead of the MAEs, the RMSEs can also be used as objective functions for the parameter identification procedure.

4.3. Parameter identification with different settings

As reference for the following investigations, the parameter identification procedure is performed for the two types of PVT collectors using the following comparison:

- Two-node model with one thermal capacity vs. two node model with two thermal capacities
- Two-step approach with separated parameter identification procedure vs. one-step approach with simultaneous parameter identification procedure of thermal and electrical parameters (only for two-node model with one thermal capacity as the model with two thermal capacities requires simultaneous parameter identification of thermal and electrical parameters due to the equality of cell and absorber temperature which is calculated within the thermal performance model)
- Electrical data sheet values vs. fit of all electrical parameters: data sheet values of the manufacturer for  $\eta_{el,ref}$  and  $\beta$ ;  $a$ ,  $b$  and  $c$  calculated with measurement data according IEC 61853-1 (if appropriate data available, else data from literature was used) or fit of the electrical parameters  $\eta_{el,ref}$ ,  $\beta$ ,  $a$ ,  $b$  and  $c$  in addition to  $U_{PVT}/U_{PVT'}$

and  $b_{0,el}$ .

In all cases, MAEs are used as objective functions and GPS-HJ as optimization algorithm.

The results of the parameter identification are summarized in Table 2 for PVT A and in Table 3 for PVT B. Depending on the used model and parameter identification approach, the  $MAE_{th}$  is between 12.74 W and 13.84 W for PVT A and between 9.34 W and 10.51 W for PVT B. The  $MAE_{el}$  reaches values between 2.35 W and 2.71 W for PVT A and between 2.27 W and 3.88 W for PVT B. In the following sections, the described approaches are compared to derive recommendations for the identification approach of the model parameters.

4.3.1. One thermal capacity vs. two thermal capacities

For PVT A, the two-node model with two thermal capacities yields a reduction of  $MAE_{th}$  between 6% and 8% compared to the model with one thermal capacity. In contrast,  $MAE_{el}$  increases by the model with two thermal capacities. For parameter identification with two electrical parameters, the increase of  $MAE_{el}$  is approximately 8%, for the identification of all electrical parameters  $MAE_{el}$  increases between 1% and 2%. Regarding the overall result ( $MAE_{th+el}$ ), the improvement is in the range of 5% and 6%.

For PVT B, in contrast, the use of two thermal capacities does not improve the model accuracy but increases the overall mean average error. For the parameter identification with electrical data sheet values, the model with two thermal capacities increases the  $MAE_{th}$  by 13%, while the  $MAE_{el}$  increases by approximately 6% compared to the results

**Table 3**  
Results of the parameter identification for PVT B.

PVT B - covered									
Two-node model w/ one thermal capacity						Two-node model w/ two thermal capacities			
Parameter	Unit	Two-step approach		One-step approach		Parameter	Unit	One-step approach	
		electrical data sheet values	fit of electrical parameters	electrical data sheet values	fit of electrical parameters			electrical data sheet values	fit of electrical parameters
$A_{PVT}$	m <sup>2</sup>	1.79 <sup>1</sup>	1.79 <sup>1</sup>	1.79 <sup>1</sup>	1.79 <sup>1</sup>	$A_{PVT}$	m <sup>2</sup>	1.79 <sup>1</sup>	1.79 <sup>1</sup>
$\eta_0$	-	0.595	0.595	0.592	0.595	$\tau\alpha$	-	0.930	0.745
$K_d$	-	0.903	0.903	0.904	0.905	$K_d$	-	0.848	0.900
$b_{0,th}$	-	0.087	0.087	0.092	0.085	$b_{0,th}$	-	0.132	0.074
$c_1$	W/(m <sup>2</sup> K)	6.032	6.032	6.022	6.023	$c_{1'}$	W/(m <sup>2</sup> K)	6.767	6.291
$c_2$	W/(m <sup>2</sup> K <sup>2</sup> )	0.035	0.035	0.035	0.034	$c_{2'}$	W/(m <sup>2</sup> K <sup>2</sup> )	0.070	0.048
$c_3$	J/(m <sup>3</sup> K)	0.0008	0.0008	0.0004	0.0140	$c_{3'}$	J/(m <sup>3</sup> K)	0.0765	0.0000
$c_4$	-	0.203	0.203	0.190	0.213	$c_{4'}$	-	0.805	0.440
$c_5$	J/(m <sup>2</sup> K)	16912	16912	16875	17031	$c_{abs}$	J/(m <sup>2</sup> K)	1575	2200
						$c_{fl}$	J/(m <sup>2</sup> K)	7100	7250
$c_6$	s/m	0.006	0.006	0.006	0.006	$c_{6'}$	s/m	0.000	0.018
$U_{PVT}$	W/(m <sup>2</sup> K)	15.11	31.10	15.10	33.10	$U_{PVT'}$	W/(m <sup>2</sup> K)	16.03	37.10
$b_{0,el}$	-	0.238	0.102	0.238	0.130	$b_{0,el}$	-	0.261	0.172
$\eta_{el,ref}$	-	0.1406 <sup>1</sup>	0.1376	0.1406 <sup>1</sup>	0.1376	$\eta_{el,ref}$	-	0.1406 <sup>1</sup>	0.1376
$\beta$	%/K	0.370 <sup>1</sup>	0.471	0.370 <sup>1</sup>	0.474	$\beta$	%/K	0.370 <sup>1</sup>	0.483
$a$	m <sup>2</sup> /W	-0.00001090 <sup>2</sup>	0.00008287	-0.00001090 <sup>2</sup>	0.00004785	$a$	m <sup>2</sup> /W	-0.00001090 <sup>2</sup>	-0.00000600
$b$	-	-0.04700 <sup>2</sup>	-0.04900	-0.04700 <sup>2</sup>	-0.04900	$b$	-	-0.04700 <sup>2</sup>	-0.05100
$c$	-	-1.400 <sup>2</sup>	-1.300	-1.400 <sup>2</sup>	-1.332	$c$	-	-1.400 <sup>2</sup>	-1.396
Results of objective functions									
$MAE_{th}$	W	9.34	9.34	9.34	9.34			10.51	9.34
$MAE_{el}$	W	3.64	2.27	3.64	2.28			3.88	2.37
$MAE_{th+el}$	W	12.98	11.61	12.98	11.62			14.39	11.71

<sup>1</sup>Values were obtained from the data sheets of the manufacturer.

<sup>2</sup>Values have been taken from Lämmle et al. (2017) as assumption.

with use of the model with one thermal capacity. The overall model error ( $MAE_{th+el}$ ) increases by approximately 11%. Regarding the fit with all electrical parameters, the  $MAE_{th}$  is nearly equal, while the increase of  $MAE_{el}$  is around 4%. The overall results show an increase of  $MAE_{th+el}$  by approximately 1%.

To sum up, both models, with one or two thermal capacities achieve a good agreement between simulation and test. Using two thermal capacities instead of one does not achieve a consistent improvement of the model accuracy. On the contrary, the use of the standardized model with one thermal capacity from ISO 9806 leads to a better comparability with solar thermal collectors and an easier interpretation of the model parameter. As a consequence, the two-node model with one thermal capacity is recommended as standard model for PVT collectors.

#### 4.3.2. Two-step vs. one-step approach

The results of the separated (two-step approach) and combined fit (one-step approach) achieve a similar model accuracy as the difference in the MAEs is negligible for both PVT A and PVT B. The deviations in the results are below 1% and there is no obvious trend regarding the effects of the combined fit on the overall result. As a consequence, it can be stated that the results of the combined fit are nearly the same as those of the separated approach and due to lower effort and time demand the combined fit (one-step approach) is preferable. This result was also expected as the thermal model results are used as input for the electrical modeling without feedback on the thermal modeling.

#### 4.3.3. Electrical data sheet values vs. fit of electrical parameters

For both PVT collectors, the parameter identification of all electrical parameters leads to an improvement in the model accuracy regarding  $MAE_{el}$ . The reduction of  $MAE_{el}$  for PVT A is between 6% and 12%. For PVT B, the improvement of  $MAE_{el}$  is even between 37% and 39%. At this, it should be pointed out that the electrical parameters  $a$ ,  $b$  and  $c$  for PVT B were taken from Lämmle et al. (2017) as assumption due to the

lack of available measurements from the manufacturer. This explains the strong improvements of the electrical results for PVT B by fitting all electrical parameters. In contrast, for PVT A these parameters were calculated based on measurements according to IEC 61853-1 provided by the manufacturer. Regarding both types of PVT collectors and the two-node model with one thermal capacity, the  $MAE_{th}$  is nearly equal for both electrical fit variations. In contrast, in case of the model with two thermal capacities the  $MAE_{th}$  can be reduced by approximately 11% for PVT B but increases by around 1% for PVT A. Due to the improvement of the electrical model accuracy, the parameter identification of all electrical parameters leads to a reduction of the overall model error  $MAE_{th+el}$  in all considered variations.

As a consequence, the fit of all electrical parameters is preferable over the parameterization with data sheet values or standard values from literature. Furthermore, this leads to the advantage that the parameterization is independent from the availability of manufacturer data which is often not provided with the required details.

#### 4.4. Model validation and summary

Based on the results of Section 4.3, the use of the following performance model and corresponding parameter identification procedure is recommended:

- two-node model with one thermal capacity
- one-step approach with combined thermal and electrical parameter identification procedure and MAEs as objective functions
- fit of the electrical parameters  $\eta_{el,ref}$ ,  $\beta$ ,  $a$ ,  $b$  and  $c$  in addition to  $U_{PVT}$  and  $b_{0,el}$ .

For the validation of the TRNSYS model and the parameter identification procedure, the PVT collectors are simulated with measurement data sets different to the data used for the parameter identification and

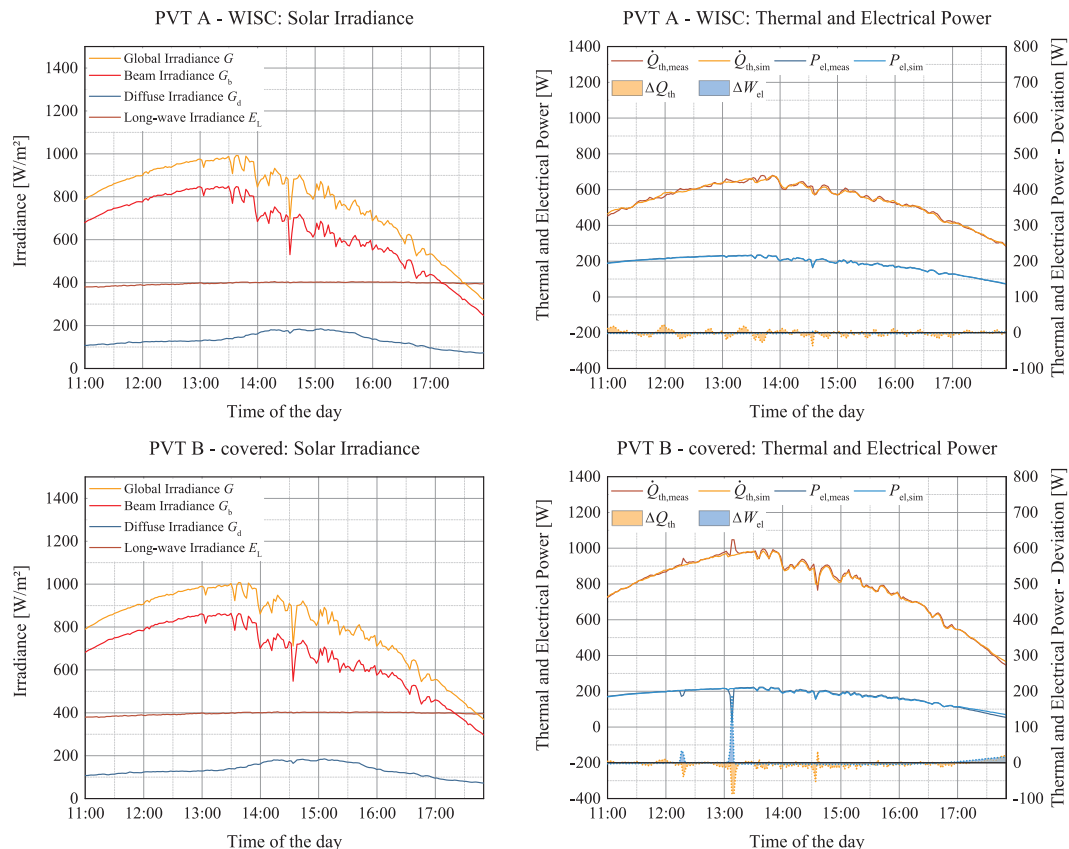


Fig. 8. Model validation – Mostly clear sky (Day type 1).

the simulation results are compared with the measured values.

The dynamic behavior of the thermal and electrical power output of the PVT collectors as well as the main solar irradiance data are shown in Fig. 8 for sequence 1 (mostly clear sky, day type 1), in Fig. 9 for sequence 2 (partly cloudy, day type 2) and in Fig. 10 for sequence 3 (mean operating temperature conditions including clear sky, day type 3b). A summary of the results including the ratio of the difference between the simulated and measured thermal ( $\Delta Q_{th}$ ) or electrical ( $\Delta W_{el}$ ) energy generation related to the measured thermal ( $Q_{th,meas}$ ) or electrical ( $W_{el,meas}$ ) energy is given in Table 4.

In case of day type 1, the simulated dynamic behavior shows a good agreement to the measured values of the thermal and electrical power output of the PVT collectors, which is also expressed in a small nRMSE<sub>th</sub> of 1.95% for PVT A and 1.17% for PVT B. The nRMSE<sub>el</sub> amounts to 0.90% for PVT A and 1.94% for PVT B. The modeled energy production over the period is also in a good accuracy with a  $\Delta Q_{th}/Q_{th,meas}$ -ratio of -0.24% for PVT A and -0.55% for PVT B and a  $\Delta W_{el}/W_{el,meas}$ -ratio of -0.64% for PVT A and +0.31% for PVT B.

For day type 2 with more dynamic behavior of the solar radiation, the differences between the measured and modelled results are higher with a nRMSE<sub>th</sub> of 9.10% for PVT A and 3.55% for PVT B as well as a nRMSE<sub>el</sub> of 5.34% for PVT A and 3.85% for PVT B. The high value for nRMSE<sub>th</sub> of PVT A for this day with considerable dynamic solar radiation may be a result of the significantly higher thermal capacity in comparison to PVT B. In case of PVT B, the result is negatively affected by malfunctions of the MPP tracking at 12:15 PM and 13:10 PM which leads to an increase of nRMSE<sub>el</sub> and nRMSE<sub>th</sub>. However, the modeled energy production over the period is still in a good accuracy with a  $\Delta Q_{th}/Q_{th,meas}$ -ratio of +2.24% for PVT A and -0.06% for PVT B and a  $\Delta W_{el}/W_{el,meas}$ -ratio of +1.32% for PVT A and +2.10% for PVT B.

For day type 3b, the behavior shows a good agreement to the measurements, except the thermal behavior of PVT A with a high

nRMSE<sub>th</sub> of 18.57%. This large relative deviation may be a result of the increasing measurement uncertainty due to the low thermal power output of the WISC and high wind speeds in the collector plane during the measurements. The nRMSE<sub>th</sub> of 1.32% for PVT B shows a better agreement. The nRMSE<sub>el</sub> of 0.66% for PVT A and 0.52% for PVT B show a high model accuracy. Despite the high nRMSE<sub>th</sub>, the modeled energy production over the period achieves a good accuracy with a  $\Delta Q_{th}/Q_{th,meas}$ -ratio of +2.37% for PVT A and -1.04% for PVT B and a  $\Delta W_{el}/W_{el,meas}$ -ratio of +0.22% for PVT A and -0.78% for PVT B.

In general, the electrical results show a better fit of the dynamic behavior than the thermal results, which is expressed in smaller values of nRMSE<sub>el</sub>. Due to its lower thermal capacity, PVT B achieves a more accurate description of the dynamic behavior than PVT A. This emphasizes the importance of an accurate fit of the thermal capacity of PVT collectors. Nevertheless, the results show a very good agreement of the modeled energy production in all investigated cases and the proposed performance model can be considered validated. As summary, the whole procedure for the PVT model parameter identification with TRNSYS and GenOpt and the model validation is summarized in Fig. 11.

### 5. Conclusions and outlook

This paper presented the model description and validation of an electrical and thermal PVT collector performance model and its implementation in TRNSYS. Two modeling approaches with one or two thermal capacities were compared for two types of PVT collectors. Furthermore, different settings for the parameter identification procedure were analyzed.

In conclusion, the two-node model with nodes of PVT cell temperature and mean fluid temperature, with one effective thermal capacity is proposed as new standard PVT performance collector model, especially due to its compliance with ISO 9806. Regarding the

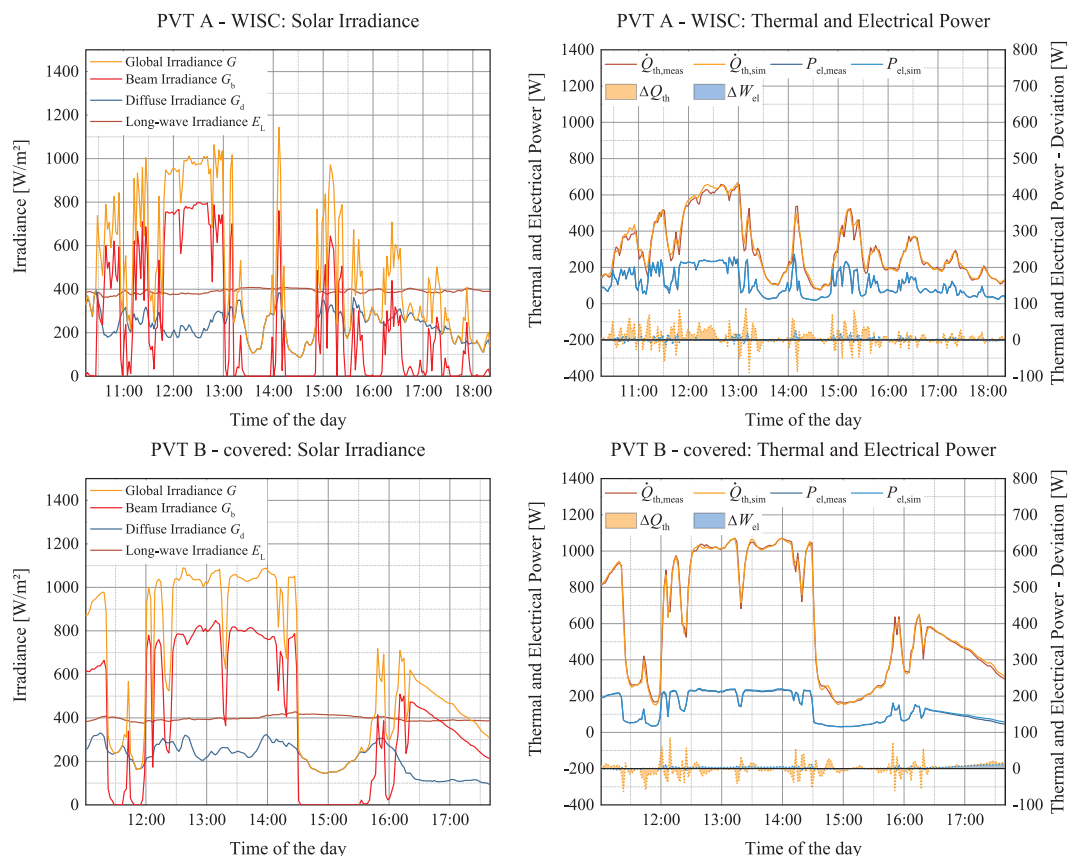


Fig. 9. Model validation – Partly cloudy (Day type 2).

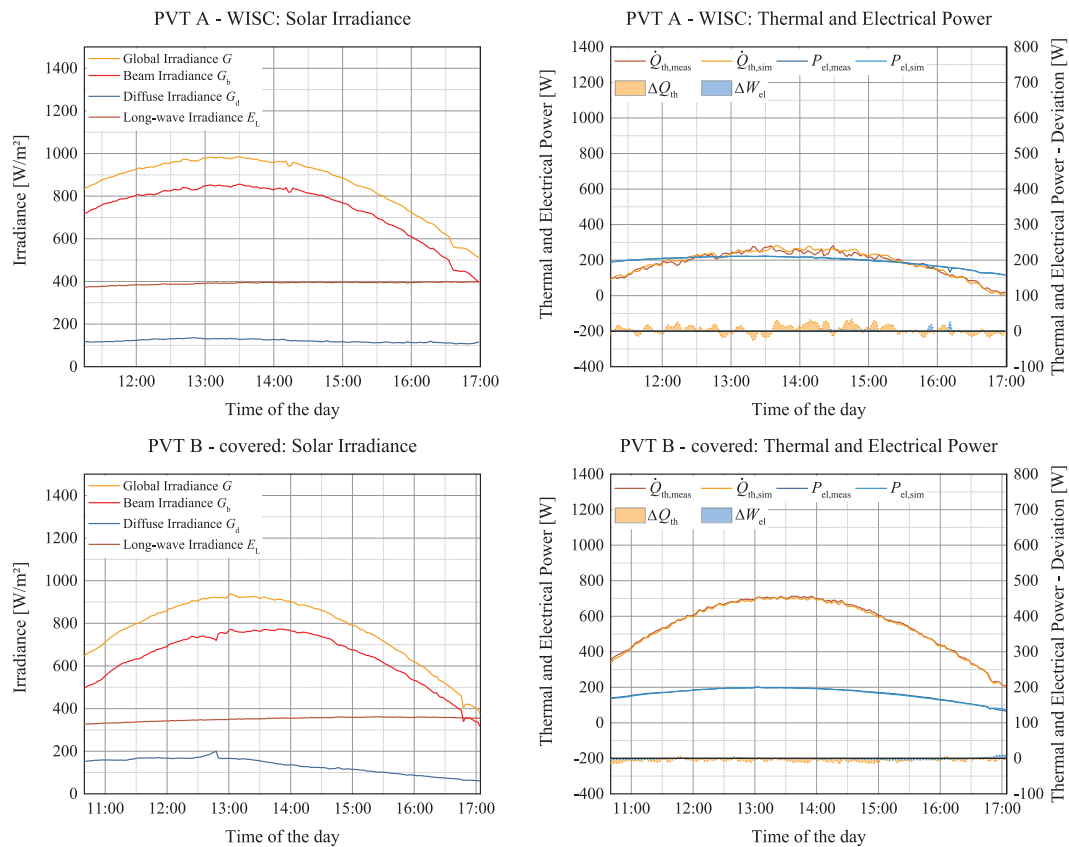


Fig. 10. Model validation – Mean operating temperature, clear sky (Day type 3b).

Table 4  
Results of the validation.

Parameter	Unit	PVT A – WISC			PVT B – covered		
		Day type 1	Day type 2	Day type 3b	Day type 1	Day type 2	Day type 3b
Day type		Day type 1	Day type 2	Day type 3b	Day type 1	Day type 2	Day type 3b
Date		16.08.2018	14.08.2018	19.08.2018	16.08.2018	04.09.2018	08.10.2018
Time period		11:00–17:56	10:15–18:21	11:15–16:59	11:00–17:50	11:01–17:39	10:40–17:04
MAE <sub>th</sub>	W	7.29	20.04	15.03	6.51	15.07	6.32
nMAE <sub>th</sub>	–	1.34%	6.62%	8.08%	0.82%	2.47%	1.14%
RMSE <sub>th</sub>	W	10.57	27.56	34.55	9.25	21.68	7.35
nRMSE <sub>th</sub>	–	1.95%	9.10%	18.57%	1.17%	3.55%	1.32%
Q <sub>th,sim</sub>	kWh	3.753	2.514	1.095	5.379	4.042	3.532
Q <sub>th,meas</sub>	kWh	3.762	2.459	1.069	5.409	4.044	3.570
ΔQ <sub>th</sub> /Q <sub>th,meas</sub>	–	–0.24%	+2.24%	+2.37%	–0.55%	–0.06%	–1.04%
MAE <sub>el</sub>	W	1.52	3.88	0.87	2.96	4.16	2.38
nMAE <sub>el</sub>	–	0.82%	3.43%	0.45%	1.71%	3.15%	1.45%
RMSE <sub>el</sub>	W	1.68	6.03	1.29	3.36	5.09	2.90
nRMSE <sub>el</sub>	–	0.90%	5.34%	0.66%	1.94%	3.85%	0.52%
W <sub>el,sim</sub>	kWh	1.283	0.928	1.118	1.184	0.893	1.044
W <sub>el,meas</sub>	kWh	1.292	0.916	1.115	1.180	0.875	1.052
ΔW <sub>el</sub> /W <sub>el,meas</sub>	–	–0.64%	+1.32%	+0.22%	+0.31%	+2.10%	–0.78%

parameter identification, a one-step approach with combined simultaneous fit of thermal and electrical parameters was identified as the most suitable method. Moreover, it is recommended to use mean average errors as objective functions and the Hooke-Jeeves optimization algorithm in GenOpt. In addition, the results showed that data sheet values of manufacturers can be used to parameterize the electrical performance model, except for the new model parameters of the internal heat transfer coefficient  $U_{PVT}$  and the electrical incidence angle modifier constant  $b_{0,el}$ . Due to the lack of availability of manufacturer data for some of the electrical parameters and as consequence of higher accuracy of the electrical model, a fit of all electrical model parameters is nevertheless preferable.

Using the identified PVT collector model parameters of the proposed parameter identification procedure with TRNSYS and GenOpt, the normalized root mean square errors of the model for the thermal part nRMSE<sub>th</sub> are between 1.95% and 18.57% for PVT A and between 1.17% and 3.55% for PVT B, depending on the day type. For the electrical part, the nRMSE<sub>el</sub> is between 0.66% and 5.34% for PVT A and between 0.52% and 3.85% for PVT B, also depending on the day type. Regarding the results, the electrical model shows a better fit of the dynamic behavior than the thermal model, which is expressed in smaller values of nRMSE<sub>el</sub>. Furthermore, it can be observed that in case of high thermal capacities (PVT A) the thermal results show a more inaccurate fit of the dynamic behavior. This emphasizes the importance of an accurate

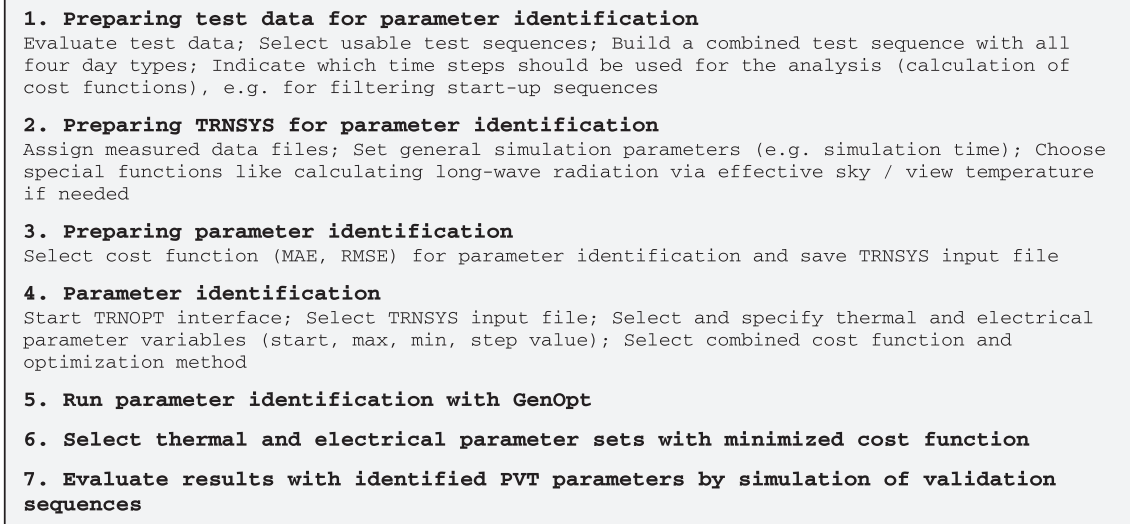


Fig. 11. Procedure for PVT model parameter identification with TRNSYS and GenOpt.

determination of the thermal capacity of PVT collectors.

Nevertheless, the results show a very good agreement of the modeled energy production in all investigated cases. This is expressed in low differences for the simulated and measured energy related to the measured values for the validation sequences that are between  $-1.04\%$  and  $+2.37\%$  for the thermal, and  $-0.78\%$  and  $+2.10\%$  for the electrical energy output. As a conclusion, the presented study pointed out that the presented PVT model and its TRNSYS implementation in Type 835 in combination with Type 832, as well as the proposed parameter identification procedure, are suitable for modeling the electrical and thermal performance of PVT collectors and that the model could be used as standardized PVT model for PVT collectors in the future.

In future work, the presented model will be used for system simulations and the comparison of the integration of different PVT collector types in solar and heat pump systems. Further improvements on the model itself should focus on the behavior in low temperature or nighttime operation and the effect of frosting and condensation gains on the thermal behavior.

## Acknowledgements

The work of Saarland University and htw saar was part of the research project SolWP-Hybrid. The project was funded by the federal state of Saarland and the European Regional Development Fund (ERDF 2014-2020). The authors are grateful for this support and thank the project partners, Viessmann Heizsysteme GmbH, Sonnenkraft GmbH and DualSun, for their support and cooperation.

## Appendix A. Supplementary material

Supplementary data to this article can be found online at <https://doi.org/10.1016/j.solener.2019.09.047>.

## References

- Almeida, P., Carvalho, M.J., Amorim, R., Mendes, J.F., Lopes, V., 2014. Dynamic testing of systems – use of TRNSYS as an approach for parameter identification. *Sol. Energy* 104, 60–70. <https://doi.org/10.1016/j.egypro.2012.11.142>.
- Bilbao, J.I., Sproul, A.B., 2015. Detailed PVT-water model for transient analysis using RC networks. *Sol. Energy* 115, 680–693. <https://doi.org/10.1016/j.solener.2015.03.003>.
- Budig, C., Orozaliiev, J., de Keizer, A.C., Kusy, O., Vajen, K., 2009. Collector parameter identification methods and their uncertainties. In: Proceedings of the ISES Solar World Congress 2009, Johannesburg, South Africa.
- Chow, T.T., 2003. Performance analysis of photovoltaic-thermal collector by explicit dynamic model. *Sol. Energy* 75 (2), 143–152. <https://doi.org/10.1016/j.solener.2003.07.001>.
- Duffie, J.A., Beckman, W.A., 2013. *Solar Engineering of Thermal Processes*, fourth ed. John Wiley & Sons, New Jersey, United States of America.
- Fischer, S., Müller-Steinhagen, H., 2009. Collector efficiency testing – the 2-node collector model ready for implementation in European Standard EN 12975. In: Proceedings of the ISES Solar World Congress 2009, Johannesburg, South Africa.
- Fischer, S., Frey, P., Drück, H., 2012. A comparison between state-of-the-art and neural network modelling of solar collectors. *Sol. Energy* 86, 3268–3277. <https://doi.org/10.1016/j.solener.2012.09.002>.
- Florschuetz, L.W., 1979. Extension of the Hottel-Whillier model to the analysis of combined photovoltaic/thermal flat plate collectors. *Sol. Energy* 22 (4), 361–366. [https://doi.org/10.1016/0038-092X\(79\)90190-7](https://doi.org/10.1016/0038-092X(79)90190-7).
- Fritzsche, U., Althaus, J., Bott, M., 2014. Qualification of PVT Collectors – Current Status. In: Proceedings of the EuroSun 2014 Conference, Aix-Les-Bains, France.
- Haller, M., Perers, B., Bales, C., Paavilainen, J., Dalibard, A., Fischer, S., Bertram, E., 2014. TRNSYS Type 832 v5.10, Dynamic Collector Model by Bengt Perers. Updated Input-Output Reference.
- Helmers, H., Kramer, K., 2013. Multi-linear performance model for hybrid (C)PVT solar collectors. *Sol. Energy* 92, 313–322. <https://doi.org/10.1016/j.solener.2013.03.003>.
- Heydenreich, W., Müller, B., Reise, C., 2008. Describing the world with three parameters: a new approach to PV module power modelling. In: Proceedings of the 23<sup>rd</sup> European Photovoltaic Solar Energy Conference and Exhibition, <https://doi.org/10.4229/23rdEUPVSEC2008-4DO.9.4>.
- Hofmann, P., Dupeyrat, P., Kramer, K., Hermann, M., Stryi-Hipp, G., 2010. Measurements and benchmark of PV-T collectors according to EN 12975 and development of a standardized measurement procedure. In: Proceedings of the EuroSun 2010 Conference, Graz, Austria.
- IEA SHC, 2018. Task 60. PVT Systems: Application of PVT Collectors and New Solutions in HVAC Systems. Official Description, International Energy Agency Solar Heating and Cooling Programme.
- IEC 61853-1, 2011. IEC 61853. Photovoltaic (PV) module performance testing and energy rating.
- ISO 9806, 2013. ISO 9806:2013 Solar energy – Solar thermal collectors – Test methods.
- ISO 9806, 2017. ISO 9806:2017 Solar energy – Solar thermal collectors – Test methods. Second edition.
- Jonas, D., 2018. DnJns/TRNSYS\_Type835\_PVT:Type835 v3.3. PV model for the coupling with solar thermal absorber and collector models as PVT model. doi: 10.5281/zenodo.1460359.
- Jonas, D., Theis, D., Frey, G., 2018. Implementation and Experimental Validation of a Photovoltaic-Thermal (PVT) Collector Model in TRNSYS. In: Proceedings of the 12th International Conference on Solar Energy for Buildings and Industry (EuroSun2018), Rapperswil, Switzerland. doi: 10.18086/eurosun2018.02.16.
- Kramer, K., Helmers, H., 2013. The interaction of standards and innovation: hybrid photovoltaic-thermal collectors. *Sol. Energy* 98 (Part C), 434–439. doi: 10.1016/j.solener.2013.08.042.
- Lämmle, M., 2018. Thermal management of PVT collectors – development and modelling of highly efficient PVT collectors with low-emissivity coatings and overheating protection. PhD thesis, Albert Ludwig University of Freiburg. doi: 10.6094/UNIFR/16446.
- Lämmle, M., Oliva, A., Hermann, M., Kramer, K., Kramer, W., 2017. PVT collector technologies in solar thermal systems: a systematic assessment of electrical and thermal yields with the novel characteristic temperature approach. *Sol. Energy* 155, 867–879. <https://doi.org/10.1016/j.solener.2017.07.015>.
- Perers, B., 1997. An improved dynamic solar collector test method for determination of non-linear optical and thermal characteristics with multiple regression. *Sol. Energy* 59, 163–178. [https://doi.org/10.1016/S0038-092X\(97\)00147-3](https://doi.org/10.1016/S0038-092X(97)00147-3).
- Perers, B., Kovacs, P., Olsson, M., Persson, M., Pettersson, U., 2012. A tool for

- standardized collector performance calculations including PVT. *Energy Proc.* 30, 1354–1364. <https://doi.org/10.1016/j.egypro.2012.11.149>.
- SKN, 2019. Solar Keymark Scheme Rules. SKN\_NO444R1, Edition 2019-03-07. Solar Keymark Network (SKN).
- Skoplaki, E., Palyvos, J., 2009. On the temperature dependence of photovoltaic module electrical performance: a review of efficiency/power correlations. *Sol. Energy* 83, 614–624. <https://doi.org/10.1016/j.solener.2008.10.008>.
- Spirkl, W., 1997. *Dynamic System Testing Program Manual. Version 2.7. InSitu Scientific Software*.
- Theis, D., Bischoff, T., Scheidhauer, T., 2009. Implementation of the 2 nodes model for the collector performance characterisation. In: *Proceedings of the 4th European Solar Thermo Energy Conference (ESTEC) 2009, Munich, Germany*.
- TRNSYS, 2015. TRNSYS – a Transient System Simulation Program, version 17.02.0005. Solar Energy Laboratory, University of Wisconsin, Madison, Wisconsin, United States of America.
- Wetter, 2016. GenOpt®. Generic Optimization Program. User Manual. Version 3.1.1, Lawrence Berkeley National Laboratory, University of California, Berkeley, California, United States of America.
- Zenhäusern, D., Bohren, A., Rommel, M., Dittmann, S., 2015. Thermische und elektrische Charakterisierung von ungedeckten PVT-Kollektoren. In: *Tagungsband 25. Symposium Thermische Solarenergie 2015. Bad Staffelstein, Germany*.
- Zondag, H.A., 2008. Flat-plate PV-Thermal collectors and systems: a review. *Renew. Sustain. Energy Rev.* 12 (4), 891–959. <https://doi.org/10.1016/j.rser.2005.12.012>.